metals

MDPI

Article

Effects of Variated Final Temperature and Workpiece Thickness for Hot Rolling of Aluminum Alloy EN AW-8011

Jakob Kraner [1], Peter Cvahte [1], Primož Šuštarič [2], Tomaž Šuštar [2], Črtomir Donik [3], Irena Paulin [3], Shae K. Kim [4] and Kyung Il Kim [4,*]

[1] Impol Aluminium Industry, Partizanska 38, 2310 Slovenska Bistrica, Slovenia; jakob.kraner@impol.si (J.K.)
[2] Centre for Computation Continuum Mechanics, C3M, Tehnološki Park 21, 1000 Ljubljana, Slovenia
[3] Institute of Metals and Technology, IMT, Lepi Pot 11, 1000 Ljubljana, Slovenia
[4] Research Institute of Advanced Manufacturing and Materials Technology, Korea Institute of Industrial Technology, Incheon 21999, Republic of Korea
* Correspondence: kandrew@kitech.re.kr

Abstract: Hot rolling in the process chain of aluminum-rolled products presents the critical element of material quality and influences productivity. To increase the letter demand modifications of hot rolling, the consequential changes of microstructure, crystallographic texture, and mechanical and formability properties must be acknowledged and consistently considered when planning the rolling process and rolled product. Achieving lower thicknesses of the hot-rolled band would enable fewer passes with cold rolling; consequently, hot rolling with the same number of passes can be completed with lower temperatures. Microstructural and texture characterizations conducted using the light microscope and scanning electron microscope, respectively, of the 3.25 mm hot-rolled band revealed that the smaller grains appeared in the center of the cross-section, unlike for the 6 mm hot-rolled band, where smaller grains were detected on the top and bottom positions of the cross-section. Furthermore, the comparison also shows that the 6 mm hot-rolled band had 64% of random texture components and 83% of recrystallized grains, whereas the proportional adjustment for the 3.25 mm hot-rolled band had 42% of random texture components and 55% of recrystallized grains. For the mechanical testing results, the elongation values in rolling and transverse directions significantly differ only in the case of a hot-rolled band of 3.25 mm. Consequently, the earing results are more than 1.5% higher for the 3.25 mm hot-rolled band, than the 6 mm hot-rolled band.

Keywords: aluminum alloy; hot rolling; simulations; metallography; mechanical properties

Citation: Kraner, J.; Cvahte, P.; Šuštarič, P.; Šuštar, T.; Donik, Č.; Paulin, I.; Kim, S.K.; Kim, K.I. Effects of Variated Final Temperature and Workpiece Thickness for Hot Rolling of Aluminum Alloy EN AW-8011. *Metals* **2023**, *13*, 1301. https://doi.org/10.3390/met13071301

Academic Editors: Daniel Casellas, Jens Hardell and Mats Oldenburg

Received: 19 June 2023
Revised: 14 July 2023
Accepted: 18 July 2023
Published: 20 July 2023

1. Introduction

Hot rolling is a process of metal forming performed above the recrystallization temperature. In the industry, there are two typical hot-rolling mills. The first option is the reverse rolling mill, often replaced with the tandem rolling mill as the second option [1]. A comparison of the hot-rolled aluminum alloy EN AW-8021B to the aforementioned two mill types results in the differences in microstructure, texture and mechanical properties. The diverse average grain size and homogeneity of the microstructure's cross-section and the texture intensity produced with hot rolling were transferred to the cold rolling process and to the final foil thickness. The performance of the hot-rolling process is essential to further improve metal-forming processes, whereby one or more intermediate annealing regimes and cold rolling—and, if needed to reach the desired properties, also the final annealing—are executed [2,3].

Numerical simulations of hot rolling for aluminum alloys assume various technological and operational parameters [4,5]. The attractiveness is often focused on the temperature, stress, strain or rolling force predictions. The influences can be observed with the various numbers of rolling passes [6,7]. More detailed analyses of hot-rolling simulations were performed by A. R. Shahani et al. [8], where the workpiece geometry, rolling force,

rolling speed, reduction (strain), initial thickness and friction coefficient were systematically changed and influentially evaluated.

The change of rolling temperature from 250 °C to 450 °C for the EN AW-7075 increased elongation (more than 10%) and ultimate tensile stress (more than 150 MPa). The described improvements were confirmed with a 50% as well an 80% reduction [9]. Besides the temperature and reduction's influence on the mechanical properties, the changed chemical compositions of EN AW-6063 were performed for hot rolling and studied by B. Byra Reddy et al. [10].

In this paper, the importance of microstructure, texture, mechanical and formability properties for hot-rolled EN AW-8011 aluminum alloy is studied in detail. The influence of temperature and reduction changes is compared between simulated and industrially produced hot rolling. Analyzing the hot-rolled band (HRB) with the light microscope (LM) and scanning electron microscope (SEM) contributes to the understanding of correlations between the fractions of random texture components and recrystallized grains according to the changing hot-rolling parameters. At the same time, mechanical testing realizes the connection between divergent elongations (A) and earing (Ea) measurements.

2. Experimental Procedure

The slabs of aluminum alloy EN AW-8011 with dimensions 490 × 1150 × 5000 mm^3 were reverse hot-rolled to the different thicknesses of the hot-rolled band (HRB). The reverse hot rolling was performed on a single stand mill. The roughing mill (reverse mill) was used, including all blocks and coiling passes, despite the possibility of using a combination of roughing mill and finishing mill (tandem mill) for block passes, with only one coiling pass, after the tandem mill. With the HRB thickness also decreased, the surface temperature of HRB after the last pass was reduced. For the 6 mm HRB, the measured temperature after hot rolling was 356 °C. The hot rolling of 3.25 mm HRB finished with a surface temperature of 320 °C. The homogenization of slabs before hot rolling was performed with the same regime. Figure 1 presents both slabs, treated with the same heating and cooling rates. After the slabs were charged in the homogenization furnace, they were heated for 8 h from approximately 275 °C to 580 °C. For the following 6 h, the temperature of the slabs' surfaces did not deviate for more than 10 °C. After the homogenization regime, the hot rolling initial temperature (500 °C) was reduced in the furnace over 3 h. Similar to the homogenization process, minor differences can be observed for the chemical compositions of 6 mm HRB and 3.25 mm HRB (Table 1). Both HRBs' chemical compositions correspond to the standard aluminum alloy EN AW-8011.

The model for numerical simulation was custom-made and validated for the two hot-rolling mills in Impol Aluminum Industry Group (Šibenik, Croatia and Sevojno, Serbia). The simulations set-up contained data of the work roll diameter (885 mm), the width of a workpiece (1150 mm) and the rolling schedule with the number of rolling passes (19) and reduction per pass to the final (exit) thickness. The number of coiling passes (3) with unwind and rewind tensions was also considered. The alloy yield curve was described with the Hansel–Spittel constitutive equation. For the material behavior during hot rolling, the density of 2613.8 $kg \cdot m^{-3}$, elastic modulus of 57,700 MPa and Poisson ratio of 0.33 were considered. The heat-transfer model functions according to the used rolled material with a thermal conductivity of 232.1 W/(m·K), specific heat of 988.8 J/(kg·°C) and linear thermal expansion of 27.2 × 10^{-6} m/(m·°C). The results of simulations were presented as a comparison of rolling force and surface temperature to the measured values during industrial hot rolling. The roll-gap visualization was used to present the last pass of hot rolling compared to the final thicknesses of 6 mm HRB and 3.25 mm HRB.

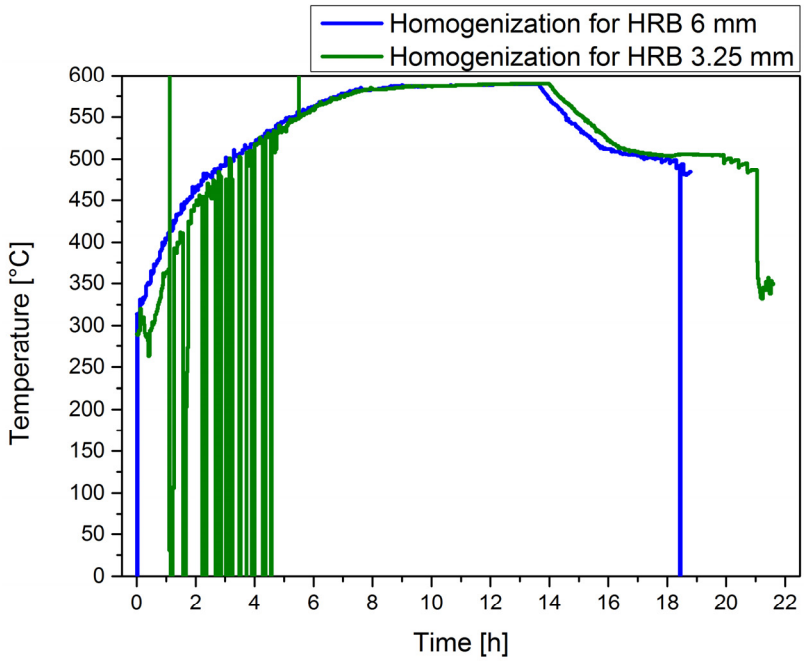

Figure 1. Graph of homogenization regime for slabs of analyzed 6 mm HRB and 3.25 mm HRB.

Table 1. Chemical composition of the analyzed material.

	Si	Fe	Mn	Mg	Cu	Ti	Al
Standard EN AW-8011	0.65–0.80	0.65–0.75	0.08–0.10	0.03–0.05	<0.1	0.02–0.04	Bal.
6 mm HRB	0.68	0.68	0.09	0.04	0.01	0.03	Bal.
3.25 mm HRB	0.68	0.67	0.09	0.04	0.01	0.02	Bal.

The metallographic preparation of the samples captures the grinding (320 grit) and polishing processes (diamond and finished, respectively, with the short time of 120 s with oxide polishing) (Struers, København, DenmarkGatan). For the light microscopy (LM), an electrolytic etching with HF (5 mL conc. HF and 100 mL H_2O) for 30 s at 40 °C, with 30 V and 0.5 mA, was used. All three sample preparation steps were executed for the scanning electron microscopy (SEM) analyses, with the replaced etching step, where the ion polishing with a PECS Gatan 628 (Gatan GmbH, Munich, Germany) for 50 min was executed. The average grain size determination was in accordance with the ASTM E112-10 (ASTM International, West Conshohocken, PA, USA). SEM analyses based on electron backscatter diffraction (EBSD) were the inverse pole figures in the Z direction (IPF-Z), and the grain average misorientation (GAM) figures were obtained. The mentioned figures enabled the detailed texture components arrangement analysis and the microstructure's recrystallized, substructured and deformed grains proportions. The GAM criteria indicate the degree of orientation uniformity within each grain. The misorientation interval was from 0° to 5°, which is the basis for the grains' state, determination and fraction of their evaluation [11–13].

Mechanical properties were measured according to ISO 6892-1:2016 (tensile test in rolling direction RD and transverse direction TD). The rectangular tension test specimens with a reduced parallel section geometry were prepared in dimensions and tolerances for standard Specimen A. The loading rate until the yield point was 10 MPa·s^{-1} (the testing velocity was 0.008 s^{-1}, which is in accordance with the testing method B). For the cup extraction, the 90 mm × 90 mm samples were taken from HRBs. The loading force was 6 kN, which is in accordance with the ISO 11531:2015 (earing test–anisotropy) standard.

For the tension test and earing measurements, the five repetitions were performed and the results are presented as their average values.

3. Results

3.1. Simulations

The simulated and industry-measured results of rolling force (Figure 2a) and surface temperature (Figure 2b) are compared between two rolling schedules for the final thicknesses of 6 mm and 3.25 mm. The deviation (around 1000 kN) at the beginning is observed, where the predicted forces with the simulations are lower than the measured forces in industrial hot rolling. The difference between measured and predicted forces is that each pass is smaller, from the seventh pass in the majority matching up to the fifteenth pass. In the industrial rolling of 3.25 mm HRB, the drop of the force is observed between the last three passes. The same is also predicted with the simulation for 3.25 mm HRB hot rolling. The rolling force in both of the final thicknesses is higher at the measured values. For the 3.25 mm HRB, the difference in rolling force for the last nineteenth pass is much smaller between the measured and predicted rolling forces than for 6 mm HRB values and simulation results. In a similar path as rolling forces, the surface's temperature differs at the beginning of hot rolling. In the comparison of temperatures, there is a deviation of 25 °C, where predicted temperatures are higher than measured. During the passes of hot rolling, the differences between measured and simulated temperatures are reduced, and after the fourteenth pass is reached, the overlapping of temperatures occurs in both cases of industrial hot rolling and simulations. For the nineteenth pass, the predicted temperatures perfectly match with the measured temperatures. The stated is observed for 6 mm HRB and 3.25 mm HRB, where the temperatures are lower as in the compared cases.

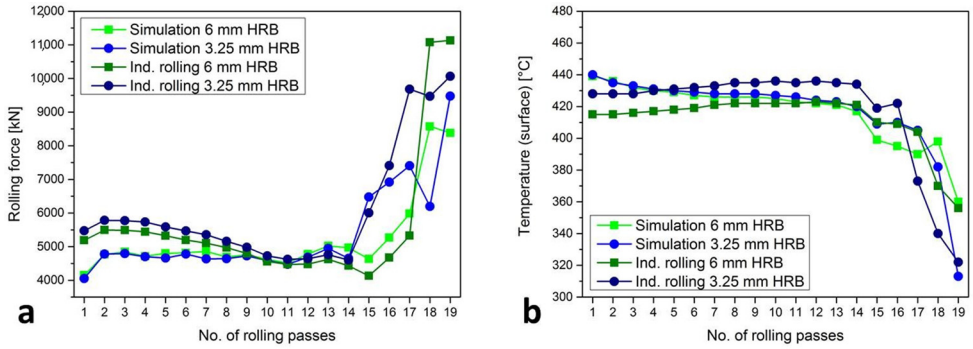

Figure 2. Comparison of 6 mm HRB and 3.25 mm HRB simulations at industrial hot rolling measured values: (**a**) rolling force; (**b**) temperature on the surface of the workpiece.

The simulation results also visualize rolling gaps (half of the workpiece). In Figure 3a, the visualization of the temperature of rolling gaps for the last hot-rolling pass is presented. It is visible that the final temperature at 6 mm HRB is higher (around 370 °C) than at 3.25 mm HRB (about 320 °C). By comparing the mentioned visualizations of rolling gaps, the entry temperature of 6 mm HRB is found to be similar to the exit temperature of 3.25 mm HRB. Figure 3b shows us the comparison of stress distribution during the last pass of hot rolling. In the center of 3.25 mm HRB, stresses are higher than 100 N/mm^2. The expected stresses for the 6 mm HRB in the center are similar to those for the 3.25 mm before the exit of a rolling gap. Furthermore, there are strain rate visualizations of rolling gaps in Figure 3c. Higher strain rate values were observed at the 3.25 mm HRB compared to the 6 mm HRB. The maximum strain rate at the 6 mm HRB is higher than 50 s^{-1} but in three small spots. For the 3.25 mm HRB, the majority strain rate is higher than 40 s^{-1}. For the aforementioned simulation (3.25 mm HRB), the strain rate in the center of the rolling gap is higher than 60 s^{-1}. The velocity of the workpiece for both of the compared HRBs is even (Figure 3d). On the entry of the rolling gap, the velocity is 1.12 m/s. The velocity of the workpiece on the exit of a rolling gap is 2.63 m/s.

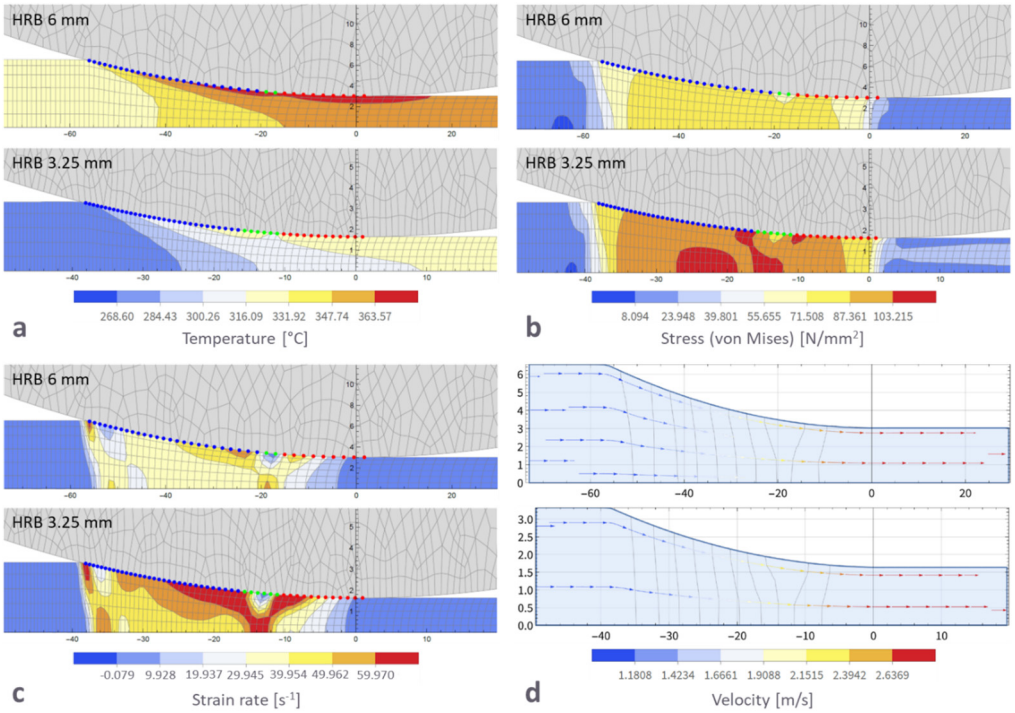

Figure 3. Visualization of rolling gaps for the last pass of hot rolling: (**a**) temperature; (**b**) von Mises stress; (**c**) strain rate; (**d**) velocity.

3.2. Metallography

The cross-section LM microstructures of compared HRBs are presented in Figure 4. In general, the microstructures of the 3.25 mm HRB have more homogeneously distributed crystal grains than for 6 mm HRB. The shape and size of crystal grains at 3.25 mm HRB are more even from the top to the bottom sample cross-section. It is also remarkable that at 6 mm HRB at the sample's edge 2, the crystal grains in the center are significantly larger than at the sample's edge 1 and center.

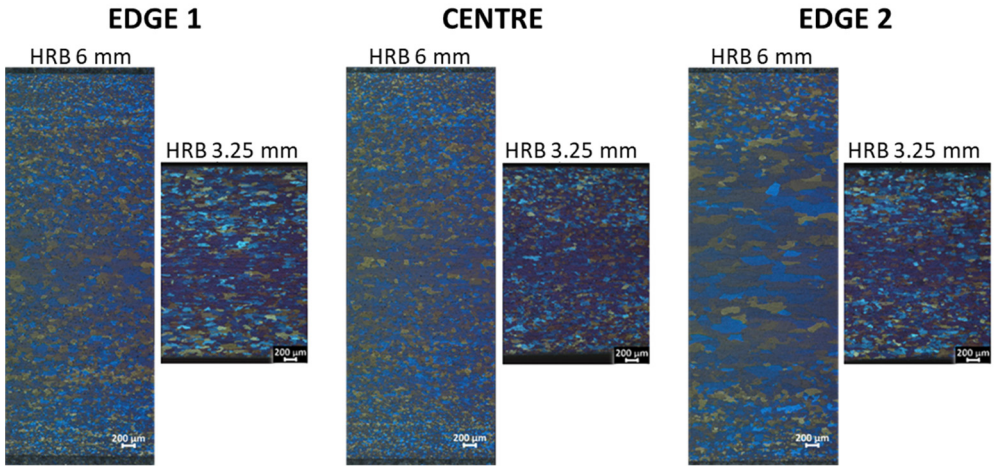

Figure 4. LM microstructures in the cross-section among the width of 6 mm HRB and 3.25 mm HRB.

The aforementioned deviation of grain size in the center of the edge 2 sample at 6 mm HRB is seen in Figure 5. IPF-Z figures from EBSD maps confirm the visual observations of LM microstructures. The top and bottom locations with the finer grain microstructure of cross-sections are more typical for the 6 mm HRB samples. At the same time, the grains in the center of the cross-section of the thicker HRB are larger than on the edges and in the center of the thinner HRB. It is important to mention that the reduction in HRB final

thickness (from 6 mm to 3.25 mm) has also resulted in some longitudinal (deformed) crystal grains in the center of all three cross-sections among the width of 3.25 mm HRB.

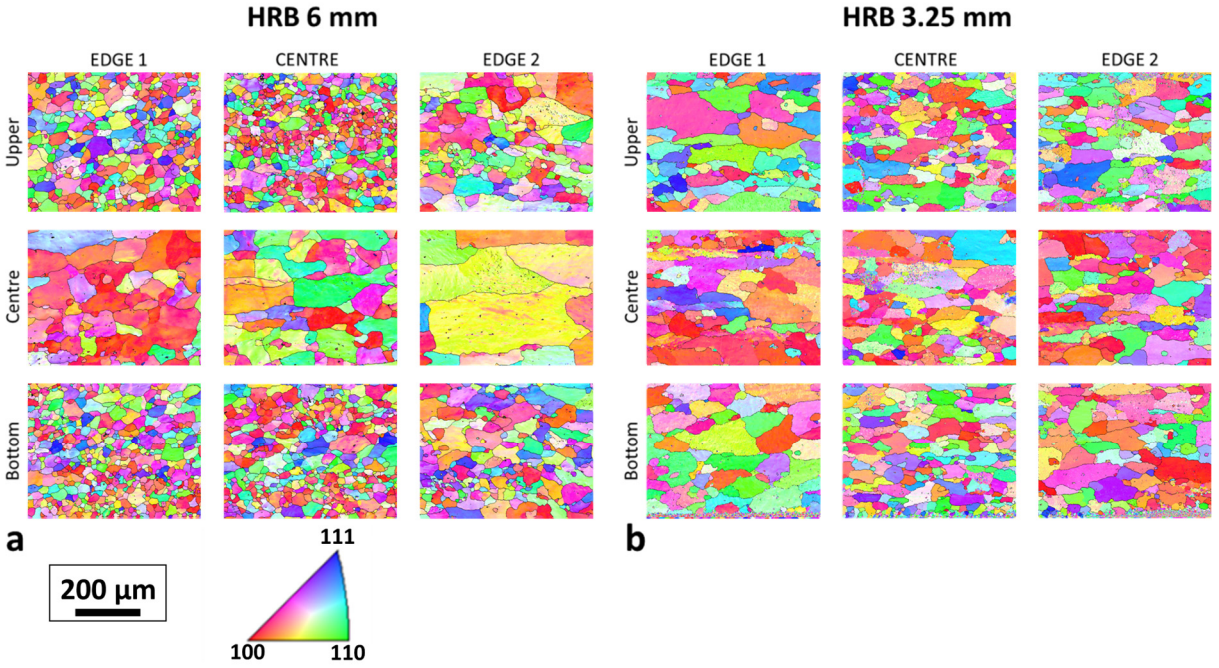

Figure 5. IPF-Z from EBSD for the samples' cross-sections: (**a**) 6 mm HRB, (**b**) 3.25 mm HRB.

The detailed results of the crystal grains' average sizes are presented in Table 2. The values of measurements with the LM and SEM-EBSD techniques are comparable and mostly deviate less than 10 µm. For the 6 mm HRB, the largest grains (213.7 µm) are in the central position of the edge 2 sample. For the 3.25 mm HRB, the largest grains (89.8 µm) were measured at the central position of the edge 1 sample. The smallest crystal grains are present at the center for both analyzed samples. The lowest value (28.3 µm) for 6 mm HRB, confirms the larger heterogeneity among the cross-sections of the thicker HRB than at the thinner HRB, where the smallest grains were 45.5 µm.

Table 2. Average crystal grain size values for 6 mm HRB and 3.25 mm HRB in the cross-section and among the total widths. Measurements were performed with the LM technique and SEM-EBSD technique.

Sample	Position	Average Crystal Grain Size Diameter (µm)			
		6 mm HRB		3.25 mm HRB	
		LM	SEM-EBSD	LM	SEM-EBSD
EDGE 1	Top	30.4	32.4	75.5	84.9
	Centre	95.4	92.5	89.8	83.4
	Bottom	32.5	29.4	63.5	82.2
CENTRE	Top	34.8	28.3	53.4	52.6
	Centre	89.8	88.2	63.5	64.9
	Bottom	30.4	32.3	53.4	45.5
EDGE 2	Top	57.4	65.4	75.5	57.4
	Centre	198.2	213.7	75.5	68.4
	Bottom	51.3	49.9	75.5	66.1

For the crystal orientation analysis, the fraction of the eight most common texture components of aluminum-rolled textures were compared for the 6 mm HRB (Figure 6a) and 3.25 mm HRB (Figure 6b). The texture components R and Cube (more than 4%) have the largest fractions at the 6 mm HRB sample. There is a smaller percentage of all the other six analyzed texture components, but with a smaller percent, which explains the 64.1% of random texture components. The random texture components value is defined and calculated as a difference of 100% and the sum of all eight analyzed texture components percentage. Compared to the 3.25 mm HRB, the sample of the random texture components is reduced by more than 20%. The increased fraction of all eight analyzed texture components contribute to this trend. Only texture components C and D have a lower fraction of 4%. Similarly at the 6 mm HRB and the 3.25 mm HRB, the texture components R and Cube are dominant. Despite the above, it is necessary to point out that at the texture of 3.25 mm HRB, the component P with around 15% is predominant.

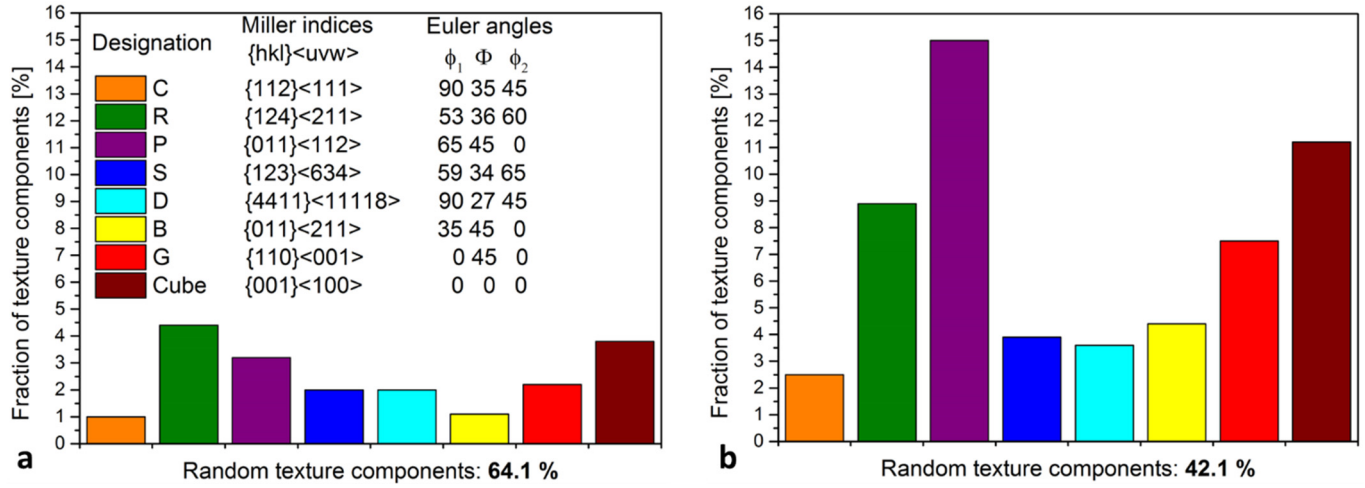

Figure 6. Fraction of texture components of SEM-EBSD analysis: (**a**) 6 mm HRB, (**b**) 3.25 mm HRB.

The share of recrystallized grains is reduced in correlation to the reduction in the random texture components with the decrease in HRB thickness from 6 mm to 3.25 mm. This is shown with the grain average misorientation (GAM) maps, where Figure 7a presents the ratio of recrystallized, substructured and deformed grains for 6 mm HRB, and Figure 7b presents the ratio of the same grains (microstructure) condition for the 3.25 mm HRB. The share of recrystallized grains is for the 6 mm HRB, around 82.8%. The percentage of substructured grains is 13.0% for the same sample, and 0.4% of grains are in the deformed condition. As previously mentioned, the share of recrystallized grains is decreased with the reduction in HRB thickness. At the same time, the percentage of substructured and deformed grains is increased. For the 3.25 mm HRB, the share of recrystallized grains is 55.2%, a percentage of 40.6% presents the substructured grains and 2.1% in the microstructure belongs to the deformed condition of grains.

3.3. Mechanical Properties and Formability

The major differences in mechanical properties between 6 mm and 3.25 mm HRBs were observed in the elongation (A) in the transverse direction (TD) according to the rolling direction (RD). There is a difference of more than 6% on the sample of edge 2, the A value is 41.0% for the 6 mm HRB and 25.8% for the 3.25 mm HRB. The interval of measured A is for the thicker HRB from 40.0% to 41.0%, although the interval of the thinner HRB is from 41.6% to the aforementioned value of 25.8%, observed for the both RD and TD directions of testing. There are also differences between Rm and Rp0.2 for the compared HRBs with different thicknesses, but the values of the mentioned properties do not differ more than 6 MPa (Table 3).

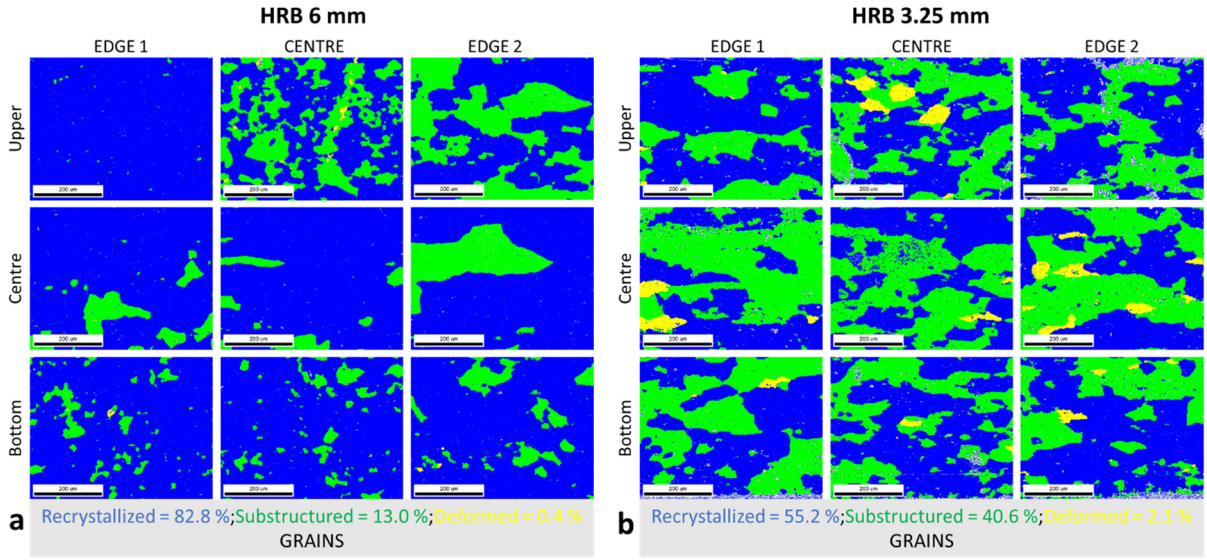

Figure 7. Grain average misorientation (GAM) maps: (**a**) 6 mm HRB, (**b**) 3.25 mm HRB.

Table 3. Mechanical properties and formability of compared 6 mm HRB and 3.25 mm HRB.

Sample	Direction	Rm (MPa)		Rp0.2 (MPa)		A (%)		Ea (%)	
		HRB 6 mm	HRB 3.25 mm	HRB 6 mm	HRB 3.25 mm	HRB 6 mm	HRB 3.25 mm	HRB 6 mm	HRB 3.25 mm
EDGE 1	RD	103	97	37	37	40.0	41.6	1.04	2.58
	TD	95	89	35	36	40.4	32.3		
CENTRE	RD	102	101	36	35	40.4	40.1	1.03	1.79
	TD	97	96	36	34	40.0	33.2		
EDGE 2	RD	102	100	36	44	40.5	39.1	1.02	2.63
	TD	95	94	35	40	41.0	25.8		

In connection to the microstructure and mechanical properties' (A) heterogeneity, the values of earing (Ea) confirm the findings. The anisotropy of 6 mm HRB is significantly lower compared to 3.25 mm HRB. The highest Ea values (2.58% and 2.63%) are presented on edge 1 and 2 positions of the 3.25 mm HRB. The trend of the higher Ea is also visible at the center position of 3.25 mm HRB. The extreme, even ($\pm$0.02) and drastically lower values (around 0.80%) are Ea values for the 6 mm HRB, which shows the lower anisotropy and homogeneity of the material (Table 3).

4. Discussion

Reducing HRB's final thickness from 6 mm to 3.25 mm contributes to fewer cold rolling passes, which decreases the operation and the wear of rolling mills. As a result, the shorter operating time of rolling mills generally allows a higher productivity. The environmental protection, besides the possibility of rolling force reduction, is also recognized with the reduced energy consumption when comparing the further cold rolling to the final foil thickness of 90 µm [14]. Comparing the technologies of cold rolling from an energy point of view revealed that the cold rolling of 3.25 mm HRB spent 53.2 kWh less power than the cold rolling of 6 mm HRB to the foil of 90 µm.

The already mentioned decrease in rolling force is also possible with asymmetric rolling [15,16]. Performing any option of asymmetry during cold rolling has peculiar microstructural, texture and technological advantages [17,18]. However, the changes and adjustments of hot rolling are easier to implement in industrial plants due to the suitability

of the rolling mill for asymmetric rolling. Further, the appearance of the ski effect with the asymmetric rolling demand to the additional operation of tensile stretch or cutting off a larger share of the rolled product reduces productivity [19].

For the special trendy foil products like coffee lids or battery foils, the characterization encompassing SEM with the EBSD technique slowly passes from merely researching and scientific approaches to the standard control techniques in the industry [20]. The requirements for the specific formability properties, less anisotropic or certain share of Cube texture components in a rolled material indicate the inability for control with the LM techniques [21]. The detailed SEM-EBSD analyses have been proven to be extremely useful with the results of random texture components and the percentage of recrystallized grains. Those results for the HRBs enable the planning of suitable technology for cold rolling. The desired mechanical and metallographic properties of foil were possible only with the assistance of HRB's properties and changes caused during hot rolling adjustments [22]. Through a further combination of mechanical properties and surface characteristics, the entire surface analysis can be performed via fracture surface parameters to identify differences caused during hot rolling [23].

The major focus for aluminum special rolled products is most often on the formability, deep-drawability and anisotropy properties, which can be connected and explained with the microstructure (grain size) and texture of material [24,25]. The reduction in the final hot-rolling temperature and thickness of HRB for the Rm and Rp0.2 measured values does not represent a key influence [26,27]. On the other hand, the mentioned two changed parameters have an effect on the A in TD and Ea values. The decrease in hot rolling temperature helped by producing the average of the smaller crystal grains, but at the same time, the increase in the share of deformed and substructured grains has the greater influence on the reduction in A values in TD [28,29]. The decrease in recrystallized grains with the smaller HRB final thickness also has a contribution to the higher anisotropy shown by Ea values [30]. The drop of recrystallized grains and especially the random texture components' share for the lower HRB thickness, which finished with the lower hot-rolling temperature, are the reason and the explanation for the higher heterogenic Ea values among the widths of rolled products [31]. The 1.5% higher Ea value for the 3.25 mm HRB compared to the 6 mm HRB can be explained with the 36 °C lower finish temperature of hot rolling for 3.25 mm HRB. The lower temperature contributes to the more texture-orientated microstructure with a lower fraction of random texture components, which, in combination with a higher share of deformed grains from the GAM criteria, tends to the more anisotropic material.

5. Conclusions

The influences of the thickness reduction and the surface temperature after the last pass of industrial hot rolling were studied on the EN AW-8011 aluminum alloy. The chemical compositions and homogenization regimes of analyzed 6 mm and 3.25 mm hot-rolled bands (HRBs) material were the same. From the combination of the simulation calculations, industrial hot-rolling and the materials characterization analysis, it can be concluded that:

- The hot rolling simulations predicted the rolling force and temperature on the surface of the workpiece for each rolling pass. Compared to the measured values of industrial hot rolling, the simulation results match to a greater extent and predict the possible intermediate deviations from increasing and decreasing trends.
- The thickness and, consequently, the temperature reduction in HRBs provide the microstructure with more evenly distributed (homogeneous) grains of a similar size through the cross-section. For the 3.25 mm HRB, the smaller grains appeared in the center of the cross-section, unlike for the 6 mm HRB, where the smaller grains were detected on the top and bottom positions of the cross-section.
- The 6 mm HRB has 64% of random texture components and 83% of recrystallized grains. The effect of temperature and thickness reduction causes the proportional

adjustment for 3.25 mm HRB, where 42% are random texture components and 55% of grains are recrystallized.

- Elongation (A) values in rolling (RD) and transverse (TD) directions significantly differ, only in the case of 3.25 mm HRB. Consequently, the earing results (Ea) are more than 1.5% higher for 3.25 mm HRB compared to 6 mm HRB.

The reduction in HRB thickness partially affects the microstructure and mechanical properties, which was also confirmed with HRB samples of intermediate 4 mm thickness. Therefore, with the aim to increase production, the technology to further improve cold rolling must be adapted while considering the microstructure, and the mechanically and thermally deviated effects.

Author Contributions: Conceptualization, J.K. and P.C.; methodology, J.K. and S.K.K.; software, P.Š. and T.Š.; validation, J.K.; formal analysis, T.Š., P.C., I.P. and Č.D.; investigation, J.K., I.P. and Č.D.; writing—original draft preparation, J.K. and K.I.K.; writing—review and editing, J.K., S.K.K. and K.I.K.; visualization, J.K. and K.I.K.; supervision, S.K.K. and K.I.K.; funding acquisition, K.I.K. All authors have read and agreed to the published version of the manuscript.

Funding: This research was supported by Ansan-Si Hidden Champion Fostering and Support project and funded by Ansan city (funding No. PIZ22220). This work was financially supported by the Slovenian Research Agency (core funding No. P2-0132).

Data Availability Statement: The data supporting the findings of this study are available within the paper.

Acknowledgments: The tool for simulating heating, hot and cold rolling was developed within the framework of the MARTINA AND MARTIN projects, which were co-financed by the Ministry of Education, Science and Sports.

Conflicts of Interest: The authors declare no conflict of interest.

Nomenclature

HRB	Hot-rolled band
SEM	Scanning electron microscopy
EBSD	Electron backscatter diffraction
IPF-Z	Inverse pole figure in Z direction
GAM	Grain average misorientation
LM	Light microscopy
Rm	Ultimate tensile strength, MPa
Rp0.2	Yield strength, MPa
A	Elongation, %
Ea	Earing measurements, %
RD	Rolling direction
TD	Transverse direction

References

1. Kraner, J.; Smolar, T.; Volšak, D.; Lažeta, M.; Skrbinek, R.; Fridrih, D.; Cvahte, P.; Godec, M.; Paulin, I. Influence of the Hot-Rolling Technique for En Aw-8021B Aluminium Alloy on the Microstructural Properties of a Cold-Rolled Foil. *Mater. Tehnol.* **2021**, *55*, 773–779. [CrossRef]
2. Zhao, Q.; Liu, Z.; Li, S.; Huang, T.; Xia, P.; Lu, L. Evolution of the Brass texture in an Al-Cu-Mg alloy during hot rolling. *J. Alloys Compd.* **2017**, *691*, 786–799. [CrossRef]
3. Maurice, C.; Driver, J.H. Hot rolling textures of aluminum. *Mater. Sci. Forum* **1994**, *157–162*, 807–812. [CrossRef]
4. Neumann, L.; Kopp, R.; Ludwig, A.; Wu, M.; Bührig-Polaczek, A.; Schneider, M.; Crumbach, M.; Gottstein, G. Simulation of casting, homogenization, and hot rolling: Consecutive process and microstructure modelling for aluminium sheet production. *Model. Simul. Mater. Sci. Eng.* **2004**, *12*, S19–S31. [CrossRef]
5. Nellippallil, A.B.; De, P.S.; Gupta, A.; Goyal, S.; Singh, A.K. Hot Rolling of a Non-heat Treatable Aluminum Alloy: Thermo-Mechanical and Microstructure Evolution Model. *Trans. Indian Inst. Met.* **2017**, *70*, 1387–1398. [CrossRef]
6. Bruni, C.; El Mehtedi, M.; Forcellese, A.; Gabrielli, F.; Simoncini, M. Simulation of multipass hot rolling of AA6082 aluminium alloy. *J. Steel Relat. Mater.* **2004**, *2*, 109–114.

7. Rudnytskyj, A.; Simon, P.; Jech, M.; Gachot, C. Constitutive modelling of the 6061 aluminium alloy under hot rolling conditions and large strain ranges. *Mater. Des.* **2020**, *190*, 108568. [CrossRef]
8. Shahani, A.R.; Setayeshi, S.; Nodamaie, S.A.; Asadi, M.A.; Rezaie, S. Prediction of influence parameters on the hot rolling process using finite element method and neural network. *J. Mater. Process. Technol.* **2009**, *209*, 1920–1935. [CrossRef]
9. Abolhasani, A.; Zarei-Hanzaki, A.; Abedi, H.R.; Rokni, M.R. The room temperature mechanical properties of hot rolled 7075 aluminum alloy. *Mater. Des.* **2012**, *34*, 631–636. [CrossRef]
10. Byra Reddy, B.; Bharathesh, T.P.; Prasad, D.S. Effect of Hot rolling on Microstructure and Mechanical behaviour of B 4 C nano particulates reinforced Al6063alloy Composites. *J. Mech. Civ. Eng.* **2021**, *18*, 53–62. [CrossRef]
11. Zheng, C.; Wang, Y.; Jin, J.; Gong, P.; Wang, X.; Wen, H.; Zhang, M. Recrystallization and grain growth behavior of variously deformed CoCrFeMnNi high-entropy alloys: Microstructure characterization and modeling. *J. Mater. Res. Technol.* **2022**, *20*, 2277–2292. [CrossRef]
12. Yoda, R.; Yokomaku, T.; Tsuji, N. Plastic deformation and creep damage evaluations of type 316 austenitic stainless steels by EBSD. *Mater. Charact.* **2010**, *61*, 913–922. [CrossRef]
13. Ghosh, S.; Patnamsetty, M.; Somani, M.C.; Peura, P. Characteristics of dynamic softening during high temperature deformation of CoCrFeMnNi high-entropy alloy and its correlation with the evolving microstructure and micro-texture. *J. Mater. Res. Technol.* **2021**, *15*, 6608–6623. [CrossRef]
14. Kraner, J.; Fajfar, P.; Palkowski, H.; Kugler, G.; Godec, M.; Paulin, I. Microstructure and texture evolution with relation to mechanical properties of compared symmetrically and asymmetrically cold rolled aluminum alloy. *Metals* **2020**, *10*, 156. [CrossRef]
15. Kraner, J.; Fajfar, P.; Palkowski, H.; Godec, M.; Paulin, I. Asymmetric cold rolling of an aa 5xxx aluminium alloy. *Mater. Tehnol.* **2020**, *54*, 575–582. [CrossRef]
16. Rudnytskyj, A.; Vorlaufer, G.; Leimhofer, J.; Jech, M.; Gachot, C. Estimating the real contact area in lubricated hot rolling ofaluminium André. *Tribiol. Int.* **2023**, *180*, 108283. [CrossRef]
17. Kraner, J.; Smolar, T.; Volsak, D.; Cvahte, P.; Godec, M.; Paulin, I. A Review of Asymmetric Rolling Osnovni Pregled Asimetričnega Valjanja. *Mater. Tehnol.* **2020**, *54*, 731–743. [CrossRef]
18. Frodal, B.H.; Thomesen, S.; Børvik, T.; Hopperstad, O.S. On fracture anisotropy in textured aluminium alloys. *Int. J. Solids Struct.* **2022**, *244–245*, 111563. [CrossRef]
19. Brun, O.; Chauveau, T.; Bacroix, B. Influence of temperature on hot rolling textures of aluminium alloys in absence of recrystallisation. *Mater. Sci. Technol.* **1991**, *7*, 167–175. [CrossRef]
20. Sidor, J.J. Effect of hot band on texture evolution and plastic anisotropy in aluminium alloys. *Metals* **2021**, *11*, 1310. [CrossRef]
21. Kraner, J.; Kevorkijan, V.; Godec, M.; Paulin, I. Metallographic Methods for Determining the Quality of Aluminium Alloys. *Mater. Tehnol.* **2021**, *55*, 541–547. [CrossRef]
22. Gravier, P.; Mas, F.; Barthelemy, A.; Boller, E.; Salvo, L.; Lhuissier, P. Pore closure in thick aluminum plate: From industrial hot rolling to individual pore observation. *J. Mater. Process. Technol.* **2022**, *303*, 117509. [CrossRef]
23. Macek, W.; Branco, R.; Szala, M.; Marciniak, Z.; Ulewicz, R.; Sczygiol, N.; Kardasz, P. Profile and areal surface parameters for fatigue fracture characterisation. *Materials* **2020**, *13*, 3691. [CrossRef] [PubMed]
24. Zhang, L.; Wang, Y.; Yang, X.; Li, K.; Ni, S.; Du, Y.; Song, M. Texture, microstructure and mechanical properties of 6111 aluminum alloy subject to rolling deformation. *Mater. Res.* **2017**, *20*, 1360–1368. [CrossRef]
25. Danilov, S.V.; Mustaeva, I.A.; Golovnin, M.A. Influence of hot rolling technological regimes on 6061 aluminium alloy sheet texture. *Solid State Phenom.* **2017**, *265*, 999–1004. [CrossRef]
26. Li, W.; Wu, M.; Xiao, D.; Huang, L.; Liu, W.; Tang, S. Effect of rolling temperature on microstructure and properties of TA31 titanium alloy hot rolled plate. *Materials* **2022**, *15*, 7517. [CrossRef]
27. Zhao, X.; Chen, L.; He, K.; Wu, N.; Zeng, J. Effect of contact heat transfer on hot rolling of aluminum alloy. *Procedia Manuf.* **2019**, *37*, 91–96. [CrossRef]
28. Wang, B.B.; Xie, G.M.; Wu, L.H.; Xue, P.; Ni, D.R.; Xiao, B.L.; Liu, Y.D.; Ma, Z.Y. Grain size effect on tensile deformation behaviors of pure aluminum. *Mater. Sci. Eng. A* **2021**, *820*, 141504. [CrossRef]
29. Skejić, D.; Dokšanović, T.; Čudina, I.; Mazzolani, F.M. The basis for reliability-based mechanical properties of structural aluminium alloys. *Appl. Sci.* **2021**, *11*, 4485. [CrossRef]
30. Hirsch, J. Texture evolution during rolling of aluminium alloys. *TMS Light Met.* **2008**, *2008*, 1071–1077.
31. Yoshida, K.; Ishizaka, T.; Kuroda, M.; Ikawa, S. The effects of texture on formability of aluminum alloy sheets. *Acta Mater.* **2007**, *55*, 4499–4506. [CrossRef]